

Analyzing velocity map images to distinguish the primary methyl photofragments from those produced upon C–Cl bond photofission in chloroacetone at 193 nm

Bridget W. Alligood, Daniel B. Straus, and Laurie J. Butler^{a)}

The James Franck Institute and Department of Chemistry, University of Chicago, Chicago, Illinois 60637, USA

(Received 9 May 2011; accepted 21 June 2011; published online 18 July 2011)

We use a combination of crossed laser-molecular beam scattering experiments and velocity map imaging experiments to investigate the three primary photodissociation channels of chloroacetone at 193 nm: C–Cl bond photofission yielding $\text{CH}_3\text{C}(\text{O})\text{CH}_2$ radicals, C–C bond photofission yielding CH_3CO and CH_2Cl products, and C– CH_3 bond photofission resulting in CH_3 and $\text{C}(\text{O})\text{CH}_2\text{Cl}$ products. Improved analysis of data previously reported by our group quantitatively identifies the contribution of this latter photodissociation channel. We introduce a forward convolution procedure to identify the portion of the signal, derived from the methyl image, which results from a two-step process in which C–Cl bond photofission is followed by the dissociation of the vibrationally excited $\text{CH}_3\text{C}(\text{O})\text{CH}_2$ radicals to $\text{CH}_3 + \text{COCH}_2$. Subtracting this from the total methyl signal identifies the methyl photofragments that result from the $\text{CH}_3 + \text{C}(\text{O})\text{CH}_2\text{Cl}$ photofission channel. We find that about 89% of the chloroacetone molecules undergo C–Cl bond photofission to yield $\text{CH}_3\text{C}(\text{O})\text{CH}_2$ and Cl products; approximately 8% result in C–C bond photofission to yield CH_3CO and CH_2Cl products, and the remaining 2.6% undergo C– CH_3 bond photofission to yield CH_3 and $\text{C}(\text{O})\text{CH}_2\text{Cl}$ products. © 2011 American Institute of Physics. [doi:10.1063/1.3609757]

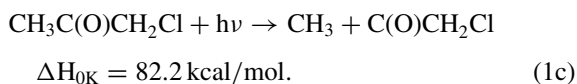
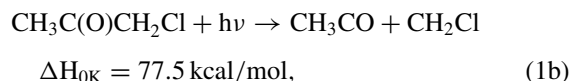
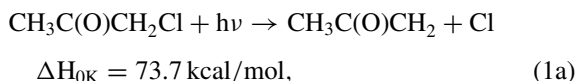
I. INTRODUCTION

The role of Cl atoms in catalyzing stratospheric ozone depletion is well known. In the troposphere, Cl atoms play a similar role to OH radicals, initiating the oxidation of volatile organic compounds, usually with larger rate constants for H-atom abstraction. For example, the rate of reaction of Cl with methane¹ is larger than that of OH with methane. Recently, Thornton *et al.*² inferred that even inland there are large sources of Cl atoms, comparable to that observed in coastal regions, suggesting that tropospheric Cl atoms arise from anthropogenic sources. Here, we focus on the photodissociation channels of chloroacetone. Originally used as a lachrymator in World War I, chloroacetone is used in a variety of industrial applications, the largest being the synthesis of drugs, perfumes, and insecticides.³

Several attempts have been made to measure the photodissociation quantum yields for the photochemistry of chloroacetone in the ultraviolet (UV). Burkholder *et al.* measured the UV absorption cross sections and photodissociation quantum yields of chloroacetone, and they also measured product quantum yields for CO, CO₂, formic acid and HCl in the bulk kinetic system at 308 and 351 nm.⁴ The primary photodissociation channels of chloroacetone could not be examined in those studies, as the primary products are radical species.

Three of our prior experiments under collision-free conditions have, however, studied the primary photofission channels. In this paper, we explicitly consider three possible

primary photodissociation channels of chloroacetone:



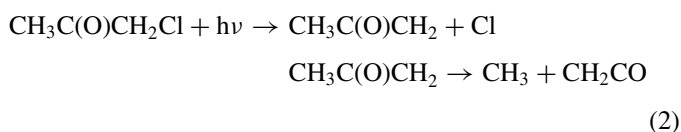
The enthalpy differences were calculated using the G3//B3LYP method, the details of which are described in the text.

Previous photodissociation studies, at 193 and 308 nm,^{5–7} definitively showed that chloroacetone exhibits the first two of these primary photofission channels – C–Cl bond photofission (Eq. (1a)) and C–C bond photofission yielding CH_3CO and CH_2Cl products (Eq. (1b)). Waschewsky *et al.*⁵ investigated the primary photofission channels of chloroacetone at 308 nm, finding that C–Cl bond fission dominated; they detected only a small contribution from aforementioned C–C photofission channel. Kitchen and co-workers later determined the branching ratio between these two photofission channels at 308 nm to be C–Cl : C–C = 4.6:1.⁶ The branching ratio that we calculated based on our previous experiments⁷ at 193 nm is larger, 11:1, showing that the relative branching to this C–C bond photofission channel decreases markedly for excitation at 193 nm. In that paper, we speculated that the 193 nm photoreactions likely proceed via excitation to the S₂ excited state,

^{a)} Author to whom correspondence should be addressed. Electronic mail: L-Butler@uchicago.edu.

followed by internal conversion to the S_1 state. If chloroacetone was analogous to acetyl chloride, in that the C–C photofission channel has a higher energetic barrier than the C–Cl photofission channel on the S_1 surface,⁸ then a statistical model would predict that the C–C photofission channel would gain importance as the excitation energy increases, not decrease as we observed. Understanding the observed product branching awaits calculations of the nonadiabatic quantum dynamics on the S_1 and S_2 excited states.

Unlike photodissociation at 308 nm, C–Cl bond photofission at 193 nm forms some $\text{CH}_3\text{C}(\text{O})\text{CH}_2$ radicals with enough internal energy to surmount the subsequent dissociation barrier to $\text{CH}_3 + \text{ketene}$, which lies 39.5 kcal/mol above the zero point energy of the $\text{CH}_3\text{C}(\text{O})\text{CH}_2$ radical. Thus, we also consider here the unimolecular dissociation of vibrationally excited $\text{CH}_3\text{C}(\text{O})\text{CH}_2$ radicals, formed in Eq. (1a) to $\text{CH}_3 + \text{ketene}$:



In our previous paper,⁷ we commented that "...the dissociating radicals produce nearly all of our CH_3 signal." We did not attempt to fit the remaining signal, emerging at faster arrival times, to CH_3 products from primary C– CH_3 bond photofission (Eq. (1c)). We detail in this paper our development of a new model, intended to fit the dissociation of the vibrationally excited $\text{CH}_3\text{C}(\text{O})\text{CH}_2$ radicals formed from C–Cl bond photofission. In applying this model, we are able to explicitly show which methyl signal is momentum-matched to the observed ketene signal, and which is not. The methyl signal that is not momentum-matched to the ketene is assigned to another photodissociation channel entirely – one that yields CH_3 and $\text{C}(\text{O})\text{CH}_2\text{Cl}$ photoproducts. Our analysis quantitatively determines the branching to this channel.

II. METHODS

A. Experimental method — Imaging apparatus

The velocity map imaging apparatus used in this work has been described previously,^{9–13} the relevant experimental conditions have also been detailed in our previous work on this system.^{7,14} We expand the molecular beam, composed of the vapor pressure of chloroacetone seeded in He to a total backing pressure of 400 Torr, through a pulsed valve; we heat the nozzle, which has a 0.8 mm diameter, to 80 °C. After passing through a skimmer, the molecules are photodissociated with a vertically polarized 193.3 nm beam.

The photofragments are ionized by 118 nm (10.5 eV) light, delayed ~ 40 ns after the photodissociation laser.¹³ The ions form a spherically expanding cloud, which travels down a grounded time-of-flight tube towards the detector. The detector consists of a position-sensitive microchannel plate assembly (MCP) coupled to a phosphor screen. We pulse the voltage on the front plate of the MCP to -750 V in order to coincide with the arrival time of ions having the desired mass-to-charge ratio. A cooled charge-coupled device camera records images

of the ions. We process the obtained images using the ion-counting method, and the raw images are symmetrized about the vertical and horizontal axes in the data analysis.

B. Experimental method – Scattering apparatus

The experimental details relevant to this system, both experimental conditions and defined apparatus parameters, have been described previously.^{7,14} We expand the molecular beam, composed of chloroacetone seeded in He to a total stagnation pressure of 400 Torr, through a continuous (not pulsed) nozzle. The nozzle has a 0.15 mm diameter, and we heat it to 180 °C. The molecular beam passes through two skimmers before it enters the main chamber, where it intersects the output of a 193.3 nm excimer laser. The molecular beam source can be rotated to different angles in the plane containing the beam and the detector axis; for the spectrum shown here, the data were acquired at a source angle of 15°. The neutral photodissociation products scatter from the interaction region with velocities determined by the vector sum of the molecular beam velocity and the recoil velocity imparted during the photodissociation. Those fragments that scatter into the detector are ionized by 200 eV electrons,¹⁵ mass-selected by a quadrupole mass spectrometer, and detected using a Daly detector.¹⁶ The signal is recorded as a function of time after the dissociating light pulse. Upon subtraction of the calibrated ion flight time, forward convolution fitting of the time-of-flight (TOF) spectrum determines the distribution of energies imparted to relative product translation during the dissociation, E_T .

C. Computational methods

The bond dissociation energies reported throughout the text are calculated with the modified G3//B3LYP method¹⁷ using the GAUSSIAN03 electronic structure package.¹⁸ We optimize the geometries using the B3LYP method with a aug-cc-pVTZ basis set and a spin-unrestricted reference. The geometries are converged to a root-mean-square (rms) force below 1×10^{-5} and a rms displacement below 4×10^{-5} , where both are in atomic units.

III. RESULTS AND ANALYSIS

A. Model for dissociation of unstable radicals

In our earlier paper,⁷ we obtained the total recoil kinetic energy distribution, $P(E_T)$, for the photoproducts resulting from a C–Cl bond photofission channel in the 193 nm photodissociation of chloroacetone (see Eq. (1a)). The bond dissociation energy, as calculated at the G3//B3LYP/aug-cc-pVTZ level of theory and reported in our previous paper, is 73.7 kcal/mol.⁷ This $P(E_T)$ was obtained via forward convolution fitting of the Cl^+ signal observed at $m/e = 35$ in the scattering apparatus with 200 eV electron bombardment ionization. In that same paper, we used the impulsive model described in Ratliff *et al.*¹⁹ and in Womack *et al.*²⁰ to predict the portion of the $\text{CH}_3\text{C}(\text{O})\text{CH}_2$ photofragments that were formed with enough vibrational energy to surmount the

dissociation barrier to CH_3 and ketene. Although stable radicals were not present at parent $m/e = 57$ ($\text{CH}_3\text{C}(\text{O})\text{CH}_2^+$) in either the scattering or imaging apparatuses, we were able to confirm the validity of the results obtained with this impulsive model by comparing with the signal observed at daughter mass-to-charge ratios – the signal observed at $m/e = 42$ (COCH_2^+) and at $m/e = 15$ (CH_3^+) in the scattering apparatus with 200 eV electron bombardment ionization,⁷ and with data taken at $m/e = 29$ (C_2H_5^+) in the imaging apparatus with 10.5 eV photoionization.¹⁴

The results from this impulsive model revealed that roughly 77.8% of the $\text{CH}_3\text{C}(\text{O})\text{CH}_2$ radicals that were formed from primary C–Cl bond photofission were stable to subsequent dissociation to CH_3 and ketene. The other 22.2% were formed with vibrational energies above the dissociation barrier out to $\text{CH}_3 + \text{ketene}$; those products were detected at $m/e = 15$ (CH_3^+) and at $m/e = 42$ (COCH_2^+), respectively. These secondary dissociation products are detected with a net velocity that is the sum of the velocities imparted during the primary C–Cl bond photofission with those velocities imparted as the CH_3 and ketene dissociate. Thus, the dissociation of these unstable radicals can be modeled as a two-step process, whereby primary C–Cl photofission is followed by dissociation of some of the $\text{CH}_3\text{C}(\text{O})\text{CH}_2$ products to ketene + CH_3 . Fitting this signal in the TOF spectrum measured in the scattering apparatus was done with a well-established forward-convolution program, CMLAB2.²¹ A comparable code is not available for velocity map imaging data.

The analysis of the velocity map imaging data presented herein, therefore, required the development of a new code beyond that usually employed in analyzing the velocity map imaging data. After ion centering,²² the primary data (a 2D image) is first processed with the usual inverse Abel transformation executed with the BASEX program.²³ The resulting 3D image gives the net velocity distribution of the detected products. After a calibrated pixel-to-speed conversion, the BASEX output reports a speed distribution $P(v) \propto \int_0^\pi I(v, \theta') v^2 \sin\theta d\theta$, and a speed-dependent anisotropy parameter, $\beta(v)$. When detecting a primary photofragment, converting the $P(v)$ to a distribution of relative kinetic energies, $P(E_T)$, imparted in the photodissociation requires only the usual Jacobian, ensuring that $P(E_T) dE_T = P(v) dv$. The methyl image analyzed here, however, includes both methyl from a primary C– CH_3 bond photofission channel in chloroacetone and from a two-step process, where primary C–Cl photofission is followed by dissociation of some of the $\text{CH}_3\text{C}(\text{O})\text{CH}_2$ products to ketene + CH_3 . The new code allows us to identify the portion of the methyl $P(v)$ due to this two-step process; we use the fact that the additional velocities imparted to the CH_3 and ketene products are momentum-matched.

The new code, given in the supplemental material,²⁴ first treats the two-step dissociation mechanism explicitly to derive, from a forward convolution fit of the measured ketene $P(v)$, the additional velocities imparted to the ketene and methyl products as the $\text{CH}_3\text{C}(\text{O})\text{CH}_2$ radicals dissociate. It then vector-sums these methyl velocities with the speeds of the dissociating radicals to predict the $P(v)$ for the methyl products from the two-step dissociation. Note that while the anisotropy in the ketene and methyl products' net velocity

distribution from this two-step mechanism depends on the anisotropy of the primary C–Cl bond photofission, the ketene and methyl products' net speed distributions do not. The input parameters are: (1) the primary C–Cl bond photofission recoil translational energy distribution, to determine the magnitude of $v_{\text{CH}_3\text{C}(\text{O})\text{CH}_2}$ for the unstable radicals; (2) the secondary distribution of recoil kinetic energies imparted as the $\text{CH}_3\text{C}(\text{O})\text{CH}_2$ radical dissociates to ketene + CH_3 (this is iterated in the forward convolution fit); (3) the angular distribution, $I(\theta)$, governing the direction of recoil of the secondary products relative to the velocity of the dissociating radical; and (4) the pairs of product masses in each step. As we do not require the net angular distribution, a simple law of cosines, with $\gamma = \pi - \theta$ to add the primary radical's speed with the secondary velocity vector of the detected fragment, allows us to calculate the net speed of the ketene or methyl product. We iteratively manipulate the secondary recoil kinetic energy (and, if needed, angular) distribution until the prediction matches our experimental data. The ketene image was well fit by using the speeds of the dissociating radicals calculated from the long-dashed line component of the C–Cl photofission $P(E_T)$ in Fig. 5 of Ref. 7 and the additional velocity imparted to the ketene products determined from the $P(E_T)$ in Fig. 12 of Ref. 7 with an isotropic $I(\theta)$. Thus, the important new information gained is the determination of the portion of the methyl $P(v)$ that is momentum-matched to the ketene in this two-step process. Subtracting that portion from the entire measured methyl $P(v)$ identifies the methyl from the C– CH_3 bond photofission channel of chloroacetone for the branching ratio determination.

B. Ketene and momentum-matched methyl from vibrationally excited $\text{CH}_3\text{C}(\text{O})\text{CH}_2$

Figure 1 shows the measured speed distribution, $P(v)$, for ketene resulting from the dissociation of vibrationally excited $\text{CH}_3\text{C}(\text{O})\text{CH}_2$, along with the fit obtained from our model which considers the two-step dissociation process explicitly. We used an isotropic angular distribution in the secondary fitting for the dissociation of the vibrationally excited radicals to $\text{CH}_3 + \text{ketene}$. The primary C–Cl bond photofission $P(E_T)$ and the secondary $P(E_T)$ for the dissociation of vibrationally excited $\text{CH}_3\text{C}(\text{O})\text{CH}_2$ radicals, as reported our earlier paper,⁷ give the net $P(v)$ shown in solid black line in Fig. 1. We note that these $P(E_T)$'s give a nearly identical fit to the TOF data as that shown in long-dashed line in the upper frame of Fig. 11 of Ref. 7. For the fits shown in that paper, we assumed that both the primary and the secondary distributions are isotropic; the range of speed-dependent anisotropies observed for the ketene signal was small, thus supporting the validity of this approximation.

The upper frame of Fig. 2 shows the portion of the observed methyl signal, obtained with the new code, that results from the dissociation of vibrationally excited $\text{CH}_3\text{C}(\text{O})\text{CH}_2$; this portion is shown in solid black line, with the total observed methyl signal given in open circles. This prediction accounts for all of the methyl that is momentum-matched to the observed ketene signal shown in Fig. 1.²⁵ With the 10.5 eV photoionization used in the imaging apparatus, we do not

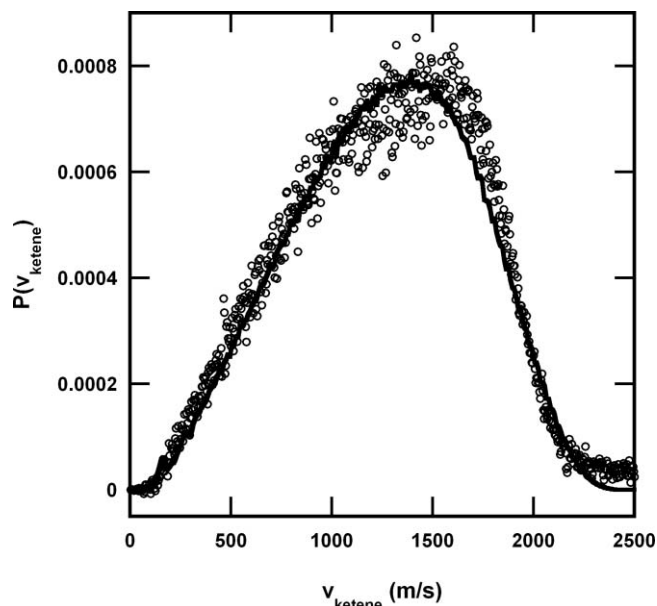


FIG. 1. Speed distribution of the ketene products as derived from the imaging data presented in Ref. 7. The open circles show the background-subtracted speed distribution of the products detected at $m/e = 42$ (COCH_2^+). The solid black line shows the fit obtained by explicitly considering both vector contributions to the observed ketene signal: the velocity imparted as the C–Cl bond breaks initially, along with the velocity imparted as the $\text{CH}_3\text{C}(\text{O})\text{CH}_2$ radical dissociates to $\text{CH}_3 + \text{ketene}$.

expect dissociative ionization of $\text{CH}_3\text{C}(\text{O})\text{CH}_2$ or CH_3CO to $m/e = 15$. Thus, the fastest methyl signal – which is not accounted for by the methyl products that are momentum-matched to the measured ketene – must be coming from another source entirely. We assign that signal, shown in solid gray line in both the upper and lower frames of Fig. 2 to primary C–CH₃ bond photofission of chloroacetone (see Eq. (1c)). The bond dissociation energy for this photodissociation channel, as calculated at the G3//B3LYP/aug-cc-pVTZ level of theory, is 82.2 kcal/mol. The resulting recoil kinetic energy distribution for this C–CH₃ bond photofission channel is shown in Fig. 3 and it extends to the energetic limit; the resulting speed distribution is shown in dotted black line in the lower frame of Fig. 2. We note that we were unable to confirm the presence of the momentum-matched $\text{C}(\text{O})\text{CH}_2\text{Cl}$ partner. It neither gave signal at parent ion in the imaging apparatus nor can we conclusively identify signal at possible daughter ions in the scattering apparatus, as the signal would be slow enough to overlap with the signal attributed to the photodissociation of molecular clusters in the beam.

In Fig. 4 we use the $P(E_T)$ in Fig. 3, assuming an isotropic angular distribution, to calculate the predicted time-of-flight (shown in solid gray line) for this additional source of methyl radicals from the minor C–CH₃ photofission channel. The fit to fast edge of the time-of-flight spectrum is much improved when this new component is added to the original fits to this spectrum detailed in Ref. 7.

C. Branching ratio for C–Cl bond photofission and C–CH₃ bond photofission forming $\text{CH}_3 + \text{C}(\text{O})\text{CH}_2\text{Cl}$

The improved analysis of this data allows us to calculate the branching ratio for C–Cl bond photofission versus

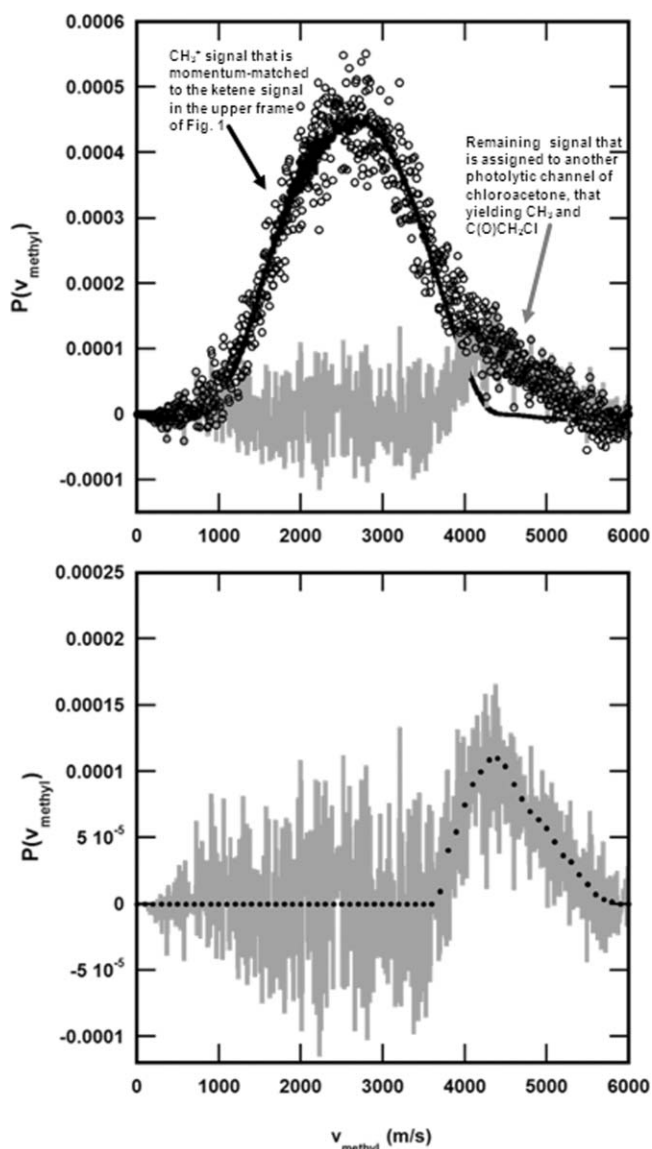


FIG. 2. Speed distribution of the CH_3 products as derived from the imaging data presented in Ref. 7, with an improved background subtraction. In the upper frame, the open circles show the background-subtracted speed distribution corresponding to all of the products detected at $m/e = 15$ (CH_3^+). The solid black line shows the signal that is momentum-matched to the ketene signal presented in Fig. 1 this is the methyl that resulted from the dissociation of vibrationally excited $\text{CH}_3\text{C}(\text{O})\text{CH}_2$ radicals. The gray line is obtained by subtracting this momentum-matched fit from the total signal. This is the signal that is attributed to another C–C bond photofission channel, C–CH₃ photofission yielding CH_3 and $\text{C}(\text{O})\text{CH}_2\text{Cl}$, as described in the text. In the lower frame, we again show in solid gray line the methyl signal attributed to C–CH₃ photofission, this time with the speed distribution, in dotted black line, calculated from the C–CH₃ photofission $P(E_T)$ in Fig. 3.

the C–CH₃ bond photofission channel described by Eq. (2), that forming $\text{CH}_3 + \text{C}(\text{O})\text{CH}_2\text{Cl}$. We saw in Sec. III B that the unstable radicals that are formed in the primary C–Cl bond photofission channel account for 22.2% of the total $\text{CH}_3\text{C}(\text{O})\text{CH}_2$ produced. We thus divide the integrated signal assigned to the dissociation of unstable $\text{CH}_3\text{C}(\text{O})\text{CH}_2$ radicals, shown in the black line in Fig. 2 by the fraction of the C–Cl bond photofission events that produced unstable radicals, thus accounting for all C–Cl bond fission, ones

that produce both stable and unstable $\text{CH}_3\text{C}(\text{O})\text{CH}_2$. Dividing this corrected integrated signal by the integrated signal for methyl formed by primary $\text{C}-\text{CH}_3$ bond photofission (under the gray line in Fig. 2) gives us the branching ratio between $\text{C}-\text{Cl}$ bond photofission and $\text{C}-\text{CH}_3$ bond photofission

$$\frac{\sigma_{\text{CH}_3\text{C}(\text{O})\text{CH}_2+\text{Cl}}}{\sigma_{\text{CH}_3+\text{COCH}_2\text{Cl}}} = \left(\frac{\text{CH}_3 \text{ signal from dissociation of unstable } \text{CH}_3\text{C}(\text{O})\text{CH}_2 \text{ radicals}}{\text{CH}_3 \text{ signal from primary } \text{C}-\text{CH}_3 \text{ photofission}} \right) \left(\frac{\text{fraction of } \text{C}-\text{Cl} \text{ bond photofission events that produce unstable } \text{CH}_3\text{C}(\text{O})\text{CH}_2 \text{ radicals}}{1} \right)$$

$$= \left(\frac{(1.81 \times 10^6 \pm 19670) / 0.222}{2.39 \times 10^5 \pm 12315} \right) = 34.1 \pm 1.8. \quad (3)$$

We assume here that the absolute photoionization cross sections of the methyl resulting from each source are similar; previous studies have shown that the vibrational dependence of the CH_3 photoionization cross section is quite weak at photoionization energies near 10.5 eV.²⁶ We also assume that, since the appearance energy of CH^+ and CH_2^+ from CH_3 are both above 15 eV,^{27,28} that we do not have to account for any dissociative ionization of methyl at 10.5 eV.

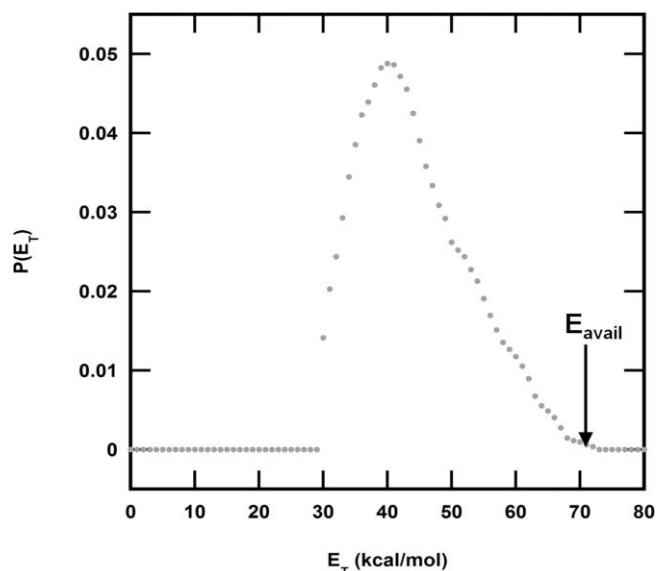


FIG. 3. Total recoil kinetic energy distribution $P(E_T)$ for the photoproducts resulting from the $\text{C}-\text{CH}_3$ bond photofission channel described by Eq. (1c); that channel results in CH_3 and $\text{C}(\text{O})\text{CH}_2\text{Cl}$ products. The resulting methyl speed distribution is shown in dotted black line in the lower frame of Fig. 2. The arrow at 70.4 kcal/mol shows the highest allowed recoil kinetic energy, E_{avail} . This value accounts for the photon energy (147.8 kcal/mol), as well as the internal energy of the chlorinated precursor (approximated as 4.8 kcal/mol in Ref. 7), and the bond dissociation energy of 82.2 kcal/mol required to break the $\text{C}-\text{CH}_3$ bond.

forming $\text{CH}_3 + \text{C}(\text{O})\text{CH}_2\text{Cl}$. The result is a branching ratio of 34.1 with a standard error of ± 1.8 , due to the error in the integrated counts estimated from the noise in the $P(v)$ data points between 2000 and 3500 m/s in the lower frame of Fig. 2 (for a confidence interval of 68%).

D. Total product branching for the three photodissociation channels of chloroacetone

The analyses described here, combined with that from our previous work, probe all of the products resulting from the 193 nm photodissociation of chloroacetone. If we assume that all of the chloroacetone molecules are undergoing one of the following four processes: (1) $\text{C}-\text{Cl}$ bond photofission to produce stable $\text{CH}_3\text{C}(\text{O})\text{CH}_2$ radicals; (2) $\text{C}-\text{Cl}$ bond

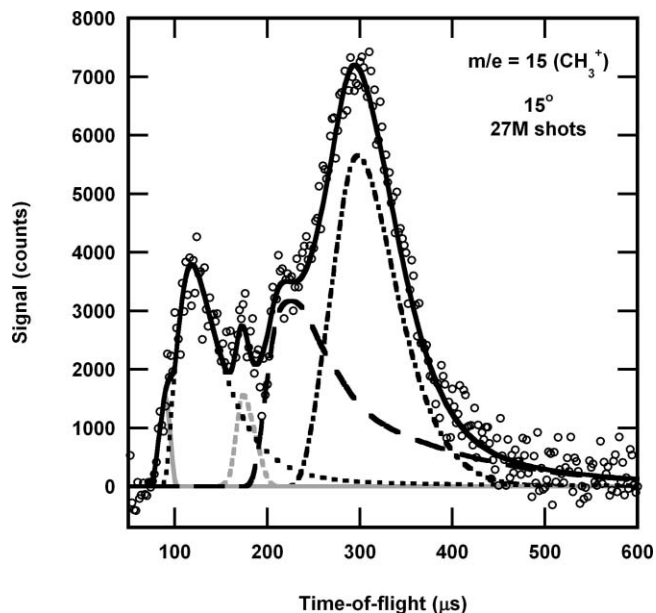


FIG. 4. Time-of-flight spectrum, reported in Ref. 7, taken at $m/e = 15$ (CH_3^+) in the scattering apparatus with 200 eV electron bombardment ionization. The new fit shown here in solid gray line, peaking at times just under 100 μs , is predicted from the $P(E_T)$ for $\text{C}-\text{CH}_3$ photofission in Fig. 3. The other fits to this TOF spectrum are detailed in the lower frame of Fig. 15 in Ref. 7. The data is shown in open circles and the overall fit to the data is shown in solid black line. The improved fit to the fast edge of the TOF spectrum shows that the imaging and scattering data are consistent with each other. (Note, this fit was not used to compute the branching fraction to the $\text{C}-\text{CH}_3$ photofission channel; that was accomplished with the methyl velocity map imaging data.)

photofission to produce vibrationally excited $\text{CH}_3\text{C}(\text{O})\text{CH}_2$ radicals that dissociate to CH_3 and ketene; (3) C–C bond photofission to yield CH_3CO and CH_2Cl ; and (4) C– CH_3 bond photofission to yield CH_3 and $\text{C}(\text{O})\text{CH}_2\text{Cl}$, then we now have enough information to calculate the absolute branching between these channels. This, of course, implies that the isomerization and subsequent dissociation of the $\text{CH}_3\text{C}(\text{O})\text{CH}_2$ radical to C_2H_5 and CO products, as discussed in Ref. 7, is negligible; this would be expected given the relative energetics for the isomerization pathway versus the direct dissociation to CH_3 and ketene.²⁹ The entire yield of photoproducts from chloroacetone photodissociation at 193 nm can thus be described as the sum of three branching fractions:

$$f_{\text{CH}_3\text{C}(\text{O})\text{CH}_2+\text{Cl}} + f_{\text{CH}_3+\text{C}(\text{O})\text{CH}_2\text{Cl}} + f_{\text{CH}_3\text{CO}+\text{CH}_2\text{Cl}} = 1, \quad (4)$$

where

$$f_{\text{CH}_3\text{C}(\text{O})\text{CH}_2+\text{Cl}} = \frac{\sigma_{\text{CH}_3\text{C}(\text{O})\text{CH}_2+\text{Cl}}}{\sigma_{\text{CH}_3\text{C}(\text{O})\text{CH}_2+\text{Cl}} + \sigma_{\text{CH}_3\text{CO}+\text{CH}_2\text{Cl}} + \sigma_{\text{CH}_3+\text{C}(\text{O})\text{CH}_2\text{Cl}}}. \quad (5)$$

Here, $f_{\text{CH}_3\text{C}(\text{O})\text{CH}_2+\text{Cl}}$ represents the fraction of chloroacetone molecules which undergo C–Cl bond fission in the photodissociation event, including those resulting in both stable and unstable $\text{CH}_3\text{C}(\text{O})\text{CH}_2$ radicals. Similarly, $f_{\text{CH}_3\text{CO}+\text{CH}_2\text{Cl}}$ is the fraction of chloroacetone molecules undergoing C–C bond photofission to yield CH_3CO and CH_2Cl , and $f_{\text{CH}_3+\text{C}(\text{O})\text{CH}_2\text{Cl}}$ is the fraction of chloroacetone molecules that undergo the C– CH_3 bond photofission channel to result in CH_3 and $\text{C}(\text{O})\text{CH}_2\text{Cl}$. Our earlier paper⁷ reported the branching ratio between C–Cl bond photofission and C–C bond photofission forming CH_3CO and CH_2Cl as

$$\frac{\sigma_{\text{CH}_3\text{C}(\text{O})\text{CH}_2+\text{Cl}}}{\sigma_{\text{CH}_3\text{CO}+\text{CH}_2\text{Cl}}} = 10.9. \quad (6)$$

Using the ratio presented in Sec. III D, along with this ratio taken from our previous publication, we can thus use Eqs. (4) and (5) to solve for the absolute branching fractions to each of these three photodissociation channels. In doing so, we get that $f_{\text{CH}_3\text{C}(\text{O})\text{CH}_2+\text{Cl}} = 0.892$, $f_{\text{CH}_3\text{CO}+\text{CH}_2\text{Cl}} = 0.082$, and $f_{\text{CH}_3+\text{C}(\text{O})\text{CH}_2\text{Cl}} = 0.026$. The uncertainties in the first two branching fractions result primarily from a $\pm 20\%$ uncertainty in the estimated electron bombardment ionization cross section, as described in Ref. 7. The standard error in the branching fraction to the C– CH_3 bond fission channel is only ± 0.002 if calculated from the error bars presented in Eq. (3), but this does not include systematic errors. A conservative estimate gives the branching fraction to the C– CH_3 photofission channel as 0.026 ± 0.005 .

IV. DISCUSSION

This work introduces a code which allows for the forward convolution fitting of speed distributions obtained from data taken with a velocity map imaging apparatus. This new code treats the secondary dissociation of vibrationally excited radi-

als explicitly; doing so allows us to identify which portion of the overall signal is from primary photofission.

We used this newly developed forward convolution program to analyze velocity map imaging data, allowing us to quantify a third primary photodissociation channel of chloroacetone at 193 nm. We found that about 89% undergo C–Cl bond photofission to yield $\text{CH}_3\text{C}(\text{O})\text{CH}_2$ and Cl products; approximately 8% result in C–C bond photofission to yield CH_3CO and CH_2Cl products, and the remaining 2.6% take part in another C–C bond photofission channel – that yielding CH_3 and $\text{C}(\text{O})\text{CH}_2\text{Cl}$ products. Although these results appear to directly correlate with the bond dissociation energies calculated at the G3//B3LYP/aug-cc-pVTZ level (as the bond dissociation energies increase, the branching to that particular photodissociation channel decreases), we note that the dynamics on the excited state are unknown, thus not allowing for any conclusions based on these energetics. The recoil kinetic energy distribution derived from fitting the primary C– CH_3 photofragment signal is peaked at high energies, near 40 kcal/mol, and extends to the energetic limit. This indicates that this channel results from dynamics on a portion of the excited state potential energy surface that is repulsive in the C– CH_3 bond near the Frank-Condon region.

ACKNOWLEDGMENTS

This work was supported by the National Science Foundation (NSF) under Grant No. CHE-0746050 (Butler).

APPENDIX: COMPUTING THE SPEED DISTRIBUTION, $P(v)$, FOR A PRODUCT OF A TWO-STEP DISSOCIATION MECHANISM

The new code we developed for this work is given in the supplemental material. It allows us to predict the net speed distribution of a fragment from a dissociation process that takes place in two steps. The output of the code is a $P(v_{1,\text{net}})$ for comparison with the $P(v)$ distribution output from BASEX (derived from velocity map imaging data). Though analogous code is routinely available for time-of-flight data in a scattering apparatus, we believe this is the first code developed to fit data taken with a velocity map imaging apparatus. The example treated in this paper is a two-step dissociation mechanism in which a chloroacetone molecule undergoes a C–Cl photofission process to make $\text{CH}_3\text{C}(\text{O})\text{CH}_2 + \text{Cl}$ ($\text{R} + \text{Cl}$) and then the radical R dissociates to $\text{CH}_3 + \text{ketene}$. The velocity of the resulting methyl is the vector sum of the velocity imparted to the radical R and the additional velocity imparted to the methyl as the radical dissociates to $\text{CH}_3 + \text{ketene}$. In this paper, the code identifies the methyl signal that is momentum-matched to the ketene produced in this two-step dissociation, so the remaining signal may be assigned to a primary C– CH_3 photofission channel.

Our program first normalizes the recoil kinetic energy distribution, $P(E_T)$, input for the primary process, the photodissociation of the C–Cl bond to form a halogen and a radical that has enough internal energy to undergo subsequent dissociation. The code uses this input $P(E_T)$ to calculate the distribution of speeds of the unstable $\text{CH}_3\text{C}(\text{O})\text{CH}_2$ radicals,

hereafter $P(v_{1,1^{\circ}})$, where $\vec{v}_{1,1^{\circ}}$ is the velocity of the primary $\text{CH}_3\text{C}(\text{O})\text{CH}_2$ radical in the center-of-mass reference frame and $v_{1,1^{\circ}}$ is the speed. The $P(E_T)$ energies are inputted in units of kcal/mol, and converted to J/molecule. The masses are entered in units of g/mol and converted to kg/molecule.

When converting the $P(E_T)$ to the $P(v_{1,1^{\circ}})$, we account for the Jacobian to assure that

$$\int_{E_a}^{E_b} P(E_T) dE_T = \int_{v_a}^{v_b} P(v_{1,1^{\circ}}) dv_{1,1^{\circ}} \quad (\text{A1})$$

as follows. Since $\vec{v}_{1,1^{\circ}}$ and $\vec{v}_{2,1^{\circ}}$ are velocities of the radical R and the momentum-matched Cl atom in the center-of-mass reference frame, with corresponding speeds v_1 and v_2 , we have

$$E_T = \frac{1}{2} \mu v_{\text{rel}}^2 = \frac{1}{2} m_1 v_1^2 + \frac{1}{2} m_2 v_2^2. \quad (\text{A2})$$

From this, we find that

$$v_1 = 100 \sqrt{\frac{2E_T}{m_1 \left(1 + \frac{m_1}{m_2}\right)}} \quad (\text{in cm/s}), \quad (\text{A3})$$

by using conservation of momentum, $m_1 \vec{v}_1 = -m_2 \vec{v}_2$, and we calculate the needed Jacobian

$$\frac{dE_T}{dv_1} = \frac{m_1 v_1 \left(1 + \frac{m_1}{m_2}\right)}{10000}, \quad (\text{A4})$$

where the factor of 10 000 is from the square of the unit conversion to cm/s.

The secondary $P(E_T)$ is converted to a $P(v_{1,2^{\circ}})$, similarly, using the input masses of CH_3 and ketene for m_1 and m_2 in this step.

The next input is a list of $I(\theta)$ and $\cos \theta$, where θ is the angle between the secondary recoil velocity, $\vec{v}_{1,2^{\circ}}$, imparted to the methyl radical as the radical R dissociates to methyl + ketene and the original velocity $\vec{v}_{1,1^{\circ}}$, of the radical R. See Fig. 5 This allows the code to easily account for the Jacobian in spherical coordinates and to normalize the distribution such that $\int_0^\pi I(\theta) \sin \theta d\theta = \int_0^\pi I(\theta) d(\cos \theta) = 1$. In an isotropic distribution, $I(\theta)$ is constant for all $\cos \theta$.

Our program then linearly interpolates between $P(v_{1,1^{\circ}})$ and $P(v_{1,2^{\circ}})$ points to allow for small increments in the primary and secondary speeds. This results in a more accurate $P(v_{1,\text{net}})$. Here, $P(v_{1,\text{net}})$ is a probability density, the distribution of net speeds of the fragment produced in the two-step dissociation. It may be directly compared to the experimental data, the $P(v)$ output by BASEX.

We note that the final speed distribution of net speeds, $P(v_{1,\text{net}})$, is insensitive to any anisotropy in the primary photodissociation. Figure 5 shows the net velocity vector will end up in the same spherical shell regardless of the direction of the original velocity $\vec{v}_{1,1^{\circ}}$; the probability of scattering into a particular spherical shell only depends on the speed $v_{1,1^{\circ}}$ imparted to R in the primary photodissociation, the speed $v_{1,2^{\circ}}$ imparted to the detected fragment in the secondary dissociation of R, and the angle between the primary and secondary dissociation vectors. We thus use the law of cosines:

$$(v_{1,\text{net}})^2 = (v_{1,1^{\circ}})^2 + (v_{1,2^{\circ}})^2 - 2v_{1,1^{\circ}}v_{1,2^{\circ}}\cos(\gamma) \quad (\text{A5})$$

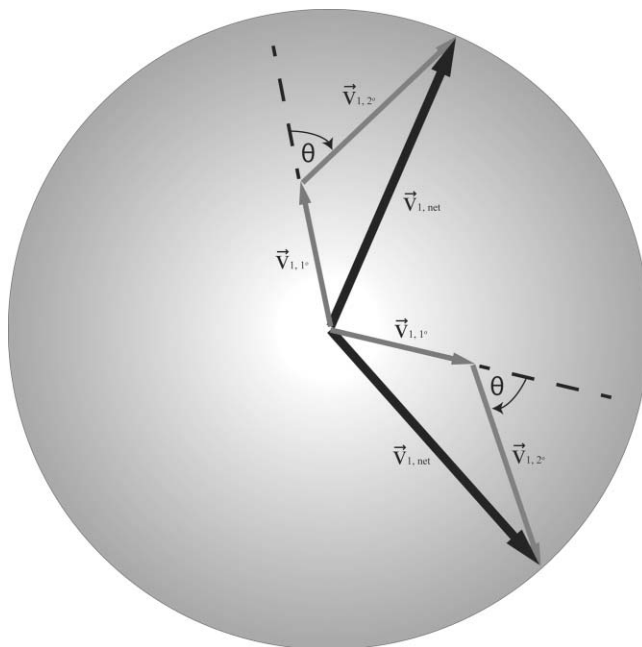


FIG. 5. Addition of velocity vectors in the center of mass reference frame for a two step dissociation mechanism (see text).

where $\gamma = \pi - \theta$. The $I(\theta)$ is thus used as the distribution of angles for the law of cosines.

To generate the $P(v_{1,\text{net}})$, our program has three nested iterative loops. It fixes a $v_{1,1^{\circ}}$ and calculates a $v_{1,\text{net}}$ for every $v_{1,2^{\circ}}$ value and $I(\theta)$ value. The contribution to the probability density $P(v_{1,\text{net}})$ for a particular combination of $v_{1,1^{\circ}}$, $v_{1,2^{\circ}}$, and $I(\theta)$ is equal to the product of the probability densities $P(v_{1,1^{\circ}}) P(v_{1,2^{\circ}}) I(\theta)$, multiplied by the increments taken in $v_{1,1^{\circ}}$, $v_{1,2^{\circ}}$, and $\cos \theta$ values in the iterative loops. The increment of $\delta \cos \theta$ in the iterative loop in $I(\theta)$ accounts for the $\sin \theta d\theta$ Jacobian in the angular distribution $I(\theta)$. We use the C library function `qsort()` to sort the net probabilities in ascending order in $v_{1,\text{net}}$, bin the probabilities into ranges $v_{1,\text{net}} + \delta v_{1,\text{net}}$, and divide by $\delta v_{1,\text{net}}$ to give a histogram of the probability density $P(v_{1,\text{net}})$. Our final distribution is thus normalized such that $\int_{v_a}^{v_b} P(v_{1,\text{net}}) dv_{1,\text{net}}$ gives the probability that the net speed $v_{1,\text{net}}$ is in the range from v_a to v_b .

To validate the new code, we compared the output to that obtained from the well-established CMLAB2 program.²¹ Figure 6 shows in solid gray line the predicted TOF spectrum, calculated with CMLAB2, of the ketene product from a two-step dissociation mechanism with an isotropic $I(\theta)$ the secondary $P(E_T)$ shown in Fig. 12 of Ref. 7. The dashed-line in Fig. 6 compares the prediction for the time-of-flight using the $P(v_{1,\text{net}})$ output by the new code assuming an isotropic angular distribution of the net speeds. They are very nearly identical. (We note that the predicted TOF obtained using CMLAB2 is potentially sensitive to any anisotropy in the primary photodissociation step of the two-step dissociation. In this system the anisotropy is small, so does not substantially affect the overall shape of the TOF distribution.)

Note, the code does not calculate the $\beta(v_{1,\text{net}})$ for comparison with that output by BASEX, and it of course assumes that all secondary recoil vectors have the same

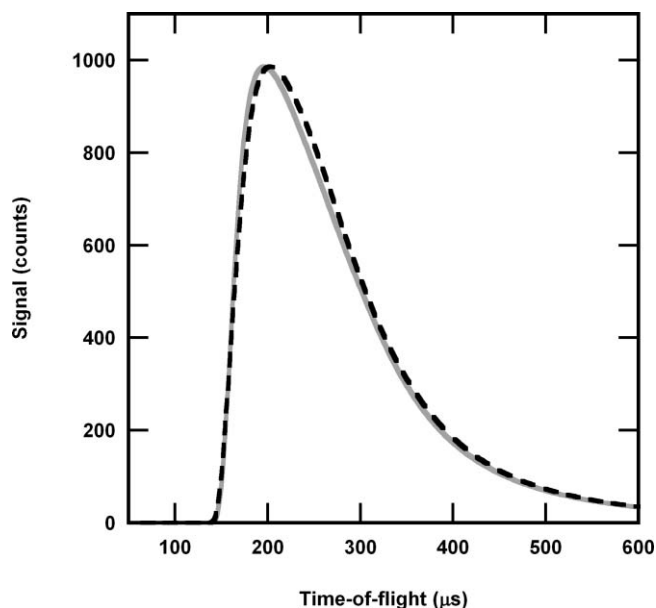


FIG. 6. Comparison of predicted TOF for code validation. The predicted time-of-flight spectrum of the ketene product from a two-step dissociation mechanism (with an isotropic $I(\theta)$ and the secondary $P(E_T)$ shown in Fig. 12 of Ref. 7) as calculated with CMLAB2 is shown in solid gray line, assuming the primary photodissociation is isotropic. The dashed-line shows the comparison, assuming an isotropic angular distribution of net speeds, with the prediction for the time-of-flight using the $P(v_{1,\text{net}})$ output for the ketene from the new code, using the same input $P(E_T)$ s and $I(\theta)$.

angular distribution $I(\theta)$. As the latter assumption is not accurate for some systems, the code can be easily modified to allow for a speed-dependent $I(\theta)$.

- ¹J. S. Pilgrim, A. McIlroy, and C. A. Taatjes, *J. Phys. Chem. A* **101**, 1873 (1997).
- ²J. A. Thornton, J. P. Kercher, T. P. Riedel, N. L. Wagner, J. Cozic, J. S. Holloway, W. P. Dubé, G. M. Wolfe, P. K. Quinn, A. M. Middlebrook, B. Alexander, and S. S. Brown, *Nature (London)* **464**, 271 (2010).
- ³*The Merck Index: An Encyclopedia of Chemicals, Drugs, and Biologicals*, edited by S. Budavari, M. O'Neill, and A. Smith, 11th ed. (Merck, Rahway, NJ, 1989).
- ⁴J. B. Burkholder, M. K. Gilles, T. Gierczak, and A. R. Ravishankara, *Geophys. Res. Lett.* **29**, 1822 (2002).
- ⁵C. Waschewsky, P. W. Kash, T. L. Myers, D. C. Kitchen, and L. J. Butler, *J. Chem. Soc., Faraday Trans.* **90**, 1581 (1994).

- ⁶D. C. Kitchen, T. L. Myers, and L. J. Butler, *J. Phys. Chem.* **100**, 5200 (1996).
- ⁷B. W. Alligood, B. L. FitzPatrick, D. E. Szpunar, and L. J. Butler, *J. Chem. Phys.* **134**, 054301 (2011).
- ⁸S.-L. Chen and W.-H. Fang, *J. Phys. Chem. A* **111**, 9355 (2007).
- ⁹A. J. R. Heck and D. W. Chandler, *Annu. Rev. Phys. Chem.* **46**, 335 (1995).
- ¹⁰A. T. J. B. Eppink and D. H. Parker, *Rev. Sci. Instrum.* **68**, 3477 (1997).
- ¹¹Y. Sato, Y. Matsumi, M. Kawasaki, K. Tsukiyama, and R. Bersohn, *J. Phys. Chem.* **99**, 16307 (1995).
- ¹²Y. Liu and L. J. Butler, *J. Chem. Phys.* **121**, 11016 (2004).
- ¹³B. J. Ratliff, X. N. Tang, L. J. Butler, D. E. Szpunar, and K.-C. Lau, *J. Chem. Phys.* **131**, 044304 (2009).
- ¹⁴B. W. Alligood, C. C. Womack, and M. D. Brynteson, *Int. J. Mass. Spectrom.* **304**, 45 (2011).
- ¹⁵Y. T. Lee, J. D. McDonald, P. R. LeBreton, and D. R. Herschbach, *Rev. Sci. Instrum.* **40**, 1402 (1969).
- ¹⁶N. R. Daly, *Rev. Sci. Instrum.* **31**, 264 (1960).
- ¹⁷A. G. Baboul, L. A. Curtiss, P. C. Redfern, and K. Raghavachari, *J. Chem. Phys.* **110**, 7650 (1999).
- ¹⁸M. J. Frisch, G. W. Trucks, H. B. Schlegel *et al.*, GAUSSIAN03, REVISION C.02, Gaussian, Inc., Pittsburgh, PA, 2003.
- ¹⁹B. J. Ratliff, C. C. Womack, X. N. Tang, W. M. Landau, L. J. Butler, and D. E. Szpunar, *J. Phys. Chem. A*, **114**, 4934 (2010).
- ²⁰C. C. Womack, W.-H. Fang, D. B. Straus, and L. J. Butler, *J. Phys. Chem. A* **114**, 13005 (2010).
- ²¹CMLAB2, version 6/93, modified by J. D. Myers. This is an interactive version built on the original cmlab2 program: X. Zhao, Ph.D. dissertation (University of California, 1988).
- ²²B. Chang, R. C. Hoetzlein, J. A. Mueller, J. D. Geiser, and P. L. Houston, *Rev. Sci. Instrum.* **69**, 1665 (1998).
- ²³V. Dribinski, A. Ossadtchi, V. A. Mandelshtam, and H. Reisler, *Rev. Sci. Instrum.* **73**, 2634 (2002).
- ²⁴See supplementary material at <http://dx.doi.org/10.1063/1.3609757> for source code.
- ²⁵Although there is potentially another energetically allowed source of methyl signal, that from the unimolecular dissociation of vibrationally excited CH_3CO photofragments formed in Eq. (1b), such signal would overlap the slower of the methyl signal that is momentum-matched to ketene. To predict the speeds of methyl from the dissociation of CH_3CO photofragments, we use the primary C–C bond fission $P(E_T)$ reported in our previous paper (Fig. 2 of Ref. 7), along with the secondary $P(E_T)$ and corresponding angular distribution for $\text{CH}_3\text{CO} \rightarrow \text{CH}_3 + \text{CO}$ as reported in Fig. 14 of S. W. North, D. A. Blank, J. D. Gezelter, C. A. Longfellow, and Y. T. Lee, *J. Chem. Phys.* **102**, 4447 (1995). Including such a contribution significantly degrades the fit (between 0 and 3500 m/s) shown in the upper frame of Fig. 2, so it is ruled out as a significant contributor.
- ²⁶C. A. Taatjes, D. L. Osborn, T. M. Selby, G. Meloni, H. Fan, and S. T. Pratt, *J. Phys. Chem. A* **112**, 9336 (2008).
- ²⁷J. D. Waldron, *Metrop. Vickers Gaz.* **27**, 66 (1956).
- ²⁸W. A. Chupka and C. Lifshitz, *J. Chem. Phys.* **48**, 1109 (1968).
- ²⁹B. L. FitzPatrick, *J. Phys. Chem. A* **115**, 1701 (2011).